Supplementary information

A tidal disruption event coincident with a high-energy neutrino

In the format provided by the authors and unedited

A tidal disruption event coincident with a high-energy neutrino - Supplementary Information

Robert Stein[*,1,2], Sjoert van Velzen[*,3,4,5], Marek Kowalski[*,1,2,6], Anna Franckowiak[1,2], Suvi Gezari[4,7], James C. A. Miller-Jones[8], Sara Frederick[4], Itai Sfaradi[9], Michael F. Bietenholz[10,11], Assaf Horesh[9], Rob Fender[12,13], Simone Garrappa[1,2], Tomás Ahumada[4], Igor Andreoni[14], Justin Belicki[15], Eric C. Bellm[16], Markus Böttcher[17], Valery Brinnel[2], Rick Burruss[15], S. Bradley Cenko[7,18], Michael W. Coughlin[19], Virginia Cunningham[4], Andrew Drake[14], Glennys R. Farrar[3], Michael Feeney[15], Ryan J. Foley[20], Avishay Gal-Yam[21], V. Zach Golkhou[16,22], Ariel Goobar[23], Matthew J. Graham[14], Erica Hammerstein[4], George Helou[24], Tiara Hung[20], Mansi M. Kasliwal[14], Charles D. Kilpatrick[20], Albert K. H. Kong[25], Thomas Kupfer[26], Russ R. Laher[24], Ashish A. Mahabal[14,27], Frank J. Masci[24], Jannis Necker[1,2], Jakob Nordin[2], Daniel A. Perley[28], Mickael Rigault[29], Simeon Reusch[1,2], Hector Rodriguez[15], César Rojas-Bravo[20], Ben Rusholme[24], David L. Shupe[24], Leo P. Singer[18], Jesper Sollerman[30], Maayane T. Soumagnac[21,31], Daniel Stern[32], Kirsty Taggart[28], Jakob van Santen[1], Charlotte Ward[4], Patrick Woudt[13], Yuhan Yao[14]

[1]*Deutsches Elektronen Synchrotron DESY, Platanenallee 6, 15738 Zeuthen, Germany*

[2]*Institut für Physik, Humboldt-Universität zu Berlin, D-12489 Berlin, Germany*

[3]*Center for Cosmology and Particle Physics, New York University, NY 10003, USA*

[4]*Department of Astronomy, University of Maryland, College Park, MD 20742, USA*

[5]*Leiden Observatory, Leiden University, PO Box 9513, 2300 RA Leiden, The Netherlands*

[6]*Columbia Astrophysics Laboratory, Columbia University in the City of New York, 550 W 120th St., New York, NY 10027, USA*

[7]*Joint Space-Science Institute, University of Maryland, College Park, MD 20742, USA*

[8]*International Centre for Radio Astronomy Research – Curtin University, Perth, Western Australia, Australia*

[9]*Racah Institute of Physics, The Hebrew University of Jerusalem, Jerusalem 91904, Israel*

[10]*Hartebeesthoek Radio Astronomy Observatory, SARAO, PO Box 443, Krugersdorp, 1740, South Africa*

[11]*Department of Physics and Astronomy, York University, Toronto, M3J 1P3, Ontario, Canada*

[12]*Astrophysics, Department of Physics, University of Oxford, Keble Road, OX1 3RH, UK*

[13]*Department of Astronomy, University of Cape Town, Private Bag X3, Rondebosch, 7701, South*

Africa

[14] *Division of Physics, Mathematics, and Astronomy, California Institute of Technology, 1200 East California Blvd, MC 249-17, Pasadena, CA 91125, USA*

[15] *Caltech Optical Observatories, California Institute of Technology, Pasadena, CA 91125, USA*

[16] *DIRAC Institute, Department of Astronomy, University of Washington, 3910 15th Avenue NE, Seattle, WA 98195, USA*

[17] *Centre for Space Research, North-West University, Potchefstroom, 2531, South Africa*

[18] *Astroparticle Physics Laboratory, NASA Goddard Space Flight Center, Mail Code 661, Greenbelt, MD 20771, USA*

[19] *School of Physics and Astronomy, University of Minnesota, Minneapolis, Minnesota 55455, USA*

[20] *Department of Astronomy and Astrophysics, University of California, Santa Cruz, California, 95064, USA*

[21] *Department of Particle Physics and Astrophysics, Weizmann Institute of Science, 234 Herzl St, Rehovot 76100, Israel*

[22] *The eScience Institute, University of Washington, Seattle, WA 98195, USA*

[23] *The Oskar Klein Centre, Department of Physics, Stockholm University, AlbaNova, SE-106 91 Stockholm, Sweden*

[24] *IPAC, California Institute of Technology, 1200 E. California Blvd, Pasadena, CA 91125, USA*

[25] *Institute of Astronomy, National Tsing Hua University, No. 101 Section 2 Kuang-Fu Road, Hsinchu 30013, Taiwan*

[26] *Kavli Institute for Theoretical Physics, University of California, Santa Barbara, CA 93106, USA*

[27] *Center for Data Driven Discovery, California Institute of Technology, Pasadena, CA 91125, USA*

[28] *Astrophysics Research Institute, Liverpool John Moores University, 146 Brownlow Hill, Liverpool L3 5RF, UK*

[29] *Université Clermont Auvergne, CNRS/IN2P3, Laboratoire de Physique de Clermont, F-63000 Clermont-Ferrand, France*

[30] *The Oskar Klein Centre, Department of Astronomy, Stockholm University, AlbaNova, SE-106 91 Stockholm, Sweden*

[31] *Lawrence Berkeley National Laboratory, 1 Cyclotron Road, Berkeley, CA 94720, USA*

[32] *Jet Propulsion Laboratory, California Institute of Technology, 4800 Oak Grove Drive, Pasadena, CA 91109, USA*

1 Discovery and Classification History of AT2019dsg

AT2019dsg was discovered by ZTF on 2019 April 9, initially named ZTF19aapreis, and reported on 2019 April 22 as a likely extragalactic transient[1]. AT2019dsg was subsequently classified as a TDE on 2019 May 13 by ePESSTO+[2]. Radio emission was tentatively reported on 2019 May 23 by AMI-LA[3], and confirmed on 2019 July 26 by e-MERLIN[4]. In addition to observations as part of a systematic ZTF search for TDEs[5], the association with IC191001A prompted additional follow-up.

2 Neutrino Production in AT2019dsg

The Hillas criterion[6] for a system of magnetic field strength B and physical radius R can be expressed as[6]:

$$\frac{E_{\max}}{\mathrm{PeV}} \approx 1600 \times \frac{B}{\mathrm{Gauss}} \times \frac{R}{10^{16}\,\mathrm{cm}} \times \beta Z \tag{1}$$

where Z is the particle charge, $\beta \sim 0.2$ is the outflow velocity in units of c and E is the maximum charged-particle energy. In order for particle acceleration to occur, the timescale required for particle acceleration must be shorter than the associated particle cooling timescale. Previous work has found this condition can be satisfied in TDEs for relevant energies[7, 8], although a detailed calculation is beyond the scope of this work.

These accelerated protons then need sufficient target density. For a photon target, with pγ pion production via the Δ resonance, we expect that neutrino production will occur above a threshold:

$$E_\gamma E_p \sim \Gamma^2 0.16\,\mathrm{GeV}^2 \tag{2}$$

With this constraint, we can derive the necessary photon energies required for a target to produce IC191001A. Taking the reconstructed neutrino energy of $\sim$0.2 PeV directly, we find a threshold photon target of $E_\gamma >$40 eV. However, these reconstructed neutrino energies typically have upper bounds an order of magnitude or more above the central estimate[9], so the true neutrino energy

3

could be substantially higher. For example, with a true neutrino energy of ~ 1 PeV, we would instead require photons $E_\gamma > 8$ eV for pion production.

During pion production roughly half of the energy will be lost through the neutrino-less π^0 channel[10], while for the charged pion channel energy is shared roughly equally among the decay products $\pi^\pm \to e^\pm + \bar{\nu}_e + \bar{\nu}_\mu + \nu_\mu$[11]. Thus $\sim 3/8$ of the pion energy is transferred to neutrinos, with a 1:2:0 flavour composition at source. However, across the cosmological baseline travelled, neutrino oscillations will lead to a mixed 1:1:1 composition on Earth. The IceCube realtime event selection is dominated by muon neutrinos, a channel which will carry no more than $\sim 1/8$ of the pionic energy. Thus we find:

$$E_\nu \approx f_\pi \frac{E_p}{8} \tag{3}$$

where $f_\pi \leq 1$ is the conversion efficiency of proton energy to pion energy. We can derive the mean free path, λ, for a proton:

$$\lambda = \frac{1}{\sigma_{p\gamma} n_\gamma} \tag{4}$$

with cross section $\sigma_{p\gamma} \sim 5 \times 10^{-28}$ cm^2 and photon number density n_γ. For a blackbody of temperature $T_{BB} \sim 10^{4.6}$ K, the mean free path for the parent proton of a 1 PeV neutrino is $\lambda \sim 2 \times 10^{13}$ cm. Accounting for the fact that each proton interaction will lead to a typical energy reduction of 20%, we then find:

$$f_\pi(x) = 1 - e^{\left(\frac{-0.2x}{\lambda}\right)} \tag{5}$$

for path x. Equating x with the radius of the UV photosphere $x \approx 10^{14.6}$cm, we then find that each proton or neutron will typically undergo ~ 10 interactions, which would represent a high efficiency $f_\pi \sim 0.9$. We caution that this estimate is only approximate, and that detailed numerical simulations are required to accurately calculate the pion production efficiency[10].

We then calculate the effective area for a single high-energy neutrino, under the assumption of a mono-energetic neutrino spectrum which approximates the expectation for pγ production.

The effective area for IceCube varies from 50-200 m^2 for a 0.2-10 PeV neutrino energy. Below 1 PeV, this corresponds to a roughly-constant threshold of 6×10^{-4} erg cm^{-2} for an expectation of one neutrino alert. Given the redshift of AT2019dsg, we find a required total energy in neutrinos $E_\nu \approx 4 \times 10^{51}$ erg to produce a single neutrino alert. We can thus express the expected number of detected neutrinos as:

$$N_\nu \approx 0.03 \times \frac{E_\nu}{10^{50}\mathrm{erg}} \tag{6}$$

This expectation would also be valid for any power-law distribution in the same energy range.

3   Compatibility with existing constraints

We can estimate the contribution of TDEs to the diffuse neutrino flux that would be required to produce an observation of one association with our ZTF follow-up program. As outlined in Table S1, a total of eight neutrino alerts were observed. For all but one of these, IceCube reported an estimate of the *signalness*, i.e., the probability for each to be astrophysical. We note that this quantity is not an absolute value, but is rather derived under specific assumptions about the underlying neutrino source population. Nonetheless, if we take these estimates at face value, and assume that the additional event had the reported signalness mean of 0.5, we would expect a total of ~4.3 astrophysical neutrinos in our sample. Taking the implied ZTF population expectation of $0.05 < N_{\nu,\mathrm{tot}} < 4.74$, we would then require that a fraction $0.01 < f < 1.00$ of the astrophysical neutrino flux was produced by ZTF-detected TDEs at 90% confidence.

We can further consider the contribution of those TDEs that ZTF has not detected, to estimate the cumulative contribution of all TDEs to the diffuse neutrino flux. The IceCube collaboration has already constrained the contribution of such TDEs to be less than 39% of the total, under the assumption of an unbroken E$^{-2.5}$ power law and a negative source evolution [12, 13]. We follow the same convention, with any power-law contribution of a transient source population to the diffuse neutrino flux is given by:
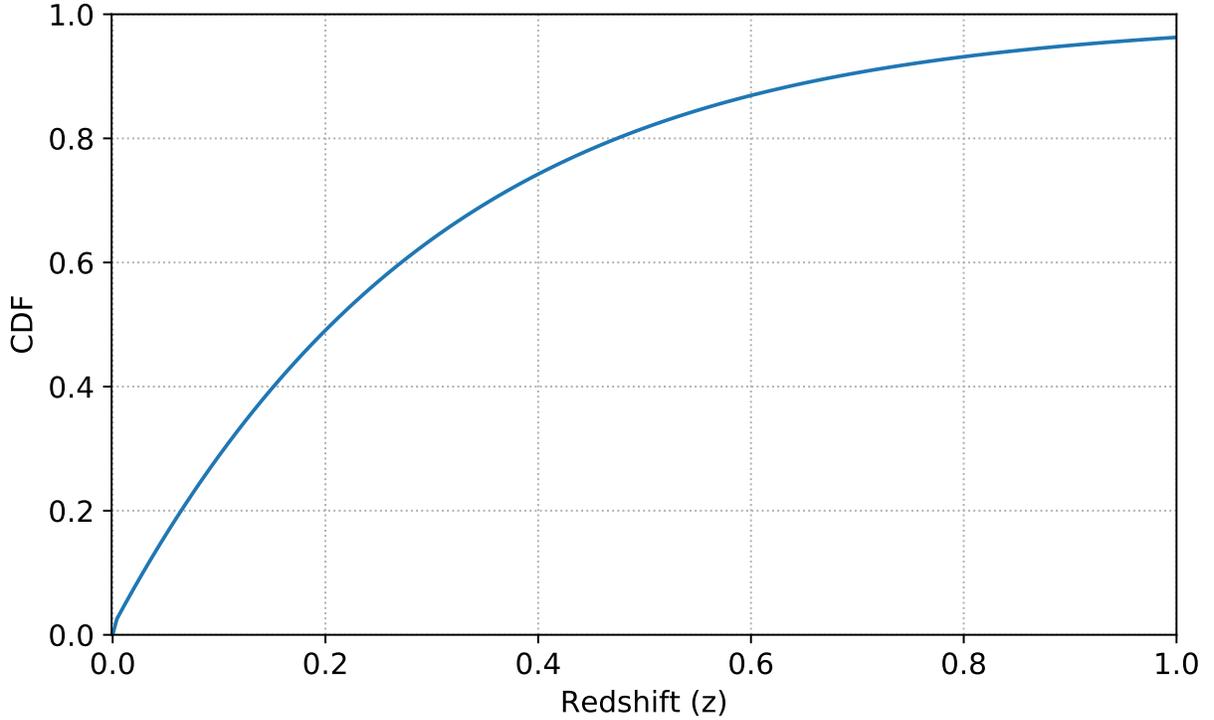
Figure S1: **Cumulative distribution function (CDF) for TDE neutrino emission as a function of redshift.** These values are derived under the assumption of an $E^{-2.5}$ power law and a negative source evolution[13]. Roughly half of all neutrinos will come from sources with $z < 0.2$.

$$\frac{dN(E, z_{max})}{dEdAdt} = \int_0^{z_{max}} \left[(1+z)^{2-\gamma} \times \frac{\rho(z)\phi_0}{4\pi D_L^2} \times \left(\frac{E}{E_0}\right)^{-\gamma} \right] \frac{dV_C}{dz} dz \qquad (7)$$

where $\rho(z)$ is the source rate density, ϕ_0 is the time-integrated particle flux normalisation at reference energy E_0. We can use this to calculate the cumulative distribution of neutrino flux as a function of redshift[14]. This CDF is illustrated in Figure S1 for an $E^{-2.5}$ power law, though the distribution only depends weakly on the assumed neutrino spectrum.

It is clear that, for this negative source evolution, the vast majority of TDE neutrinos are expected to arrive from sources in the local universe. This statement is independent of both the overall level of TDE neutrino production and the absolute TDE rate. ZTF has, thus far, reported the detection of TDEs up to a maximum redshift 0.212[5]. If we simply assume that ZTF can routinely

detect TDEs up to a redshift of 0.15, fully 40% of the total population flux should come from ZTF-detected sources. We would thus require that at least 2.8% of the astrophysical neutrino alerts are produced by TDEs, which is fully compatible with the previous IceCube limit. TDE-neutrino associations can thus be detected even if the vast majority of the astrophysical neutrino flux is produced by other source classes. The large relative contribution of detectable TDEs to the population neutrino flux is in marked contrast to supernova-like populations which are dominated by distant sources[15], so follow-up searches for TDEs are significantly more sensitive than for these other potential sources.

In any case, IceCube limits are derived under the assumptions of unbroken power laws which extend across a broad energy range (100 GeV - 10 PeV), where many additional neutrinos would be expected at lower energies. However, for the case of neutrino spectra dominated by high-energy components (as expected for pγ neutrino production), no such low-energy neutrinos would be expected, and these existing constraints would then be substantially weakened.

Supplementary References

1. Nordin, J. et al. ZTF Transient Discovery Report for 2019-04-22. *Transient Name Server Discovery Report* **2019-615** 1 (2019).

2. Nicholl, M. et al. ePESSTO+ classification of optical transients. *The Astronomer's Telegram* **12752** 1 (2019).

3. Sfaradi, I. et al. A possible radio detection of the TDE candidate AT2019DSG by AMI-LA. *The Astronomer's Telegram* **12798** 1 (2019).

4. Perez-Torres, M. et al. Unambiguous radio detection of the tidal disruption event AT2019dsg with e-MERLIN. *The Astronomer's Telegram* **12960** 1 (2019).

5. van Velzen, S. et al. Seventeen Tidal Disruption Events from the First Half of ZTF Survey Observations: Entering a New Era of Population Studies. *arXiv e-prints* arXiv:2001.01409 (2020).

6. Hillas, A.M. The Origin of Ultra-High-Energy Cosmic Rays. *Annu. Rev. Astron. Astrophys.* **22** 425–444 (1984).

7. Senno, N., Murase, K. & Mészáros, P. High-energy Neutrino Flares from X-Ray Bright and Dark Tidal Disruption Events. *Astrophys. J.* **838** 3 (2017).

8. Lunardini, C. & Winter, W. High energy neutrinos from the tidal disruption of stars. *Phys. Rev. D* **95** 123001 (2017).

9. IceCube Collaboration et al. Multimessenger observations of a flaring blazar coincident with high-energy neutrino IceCube-170922A. *Science* **361** eaat1378 (2018).

10. Hümmer, S., Rüger, M., Spanier, F. & Winter, W. Simplified Models for Photohadronic Interactions in Cosmic Accelerators. *Astrophys. J.* **721** 630–652 (2010).

11. Waxman, E. & Bahcall, J. High energy neutrinos from astrophysical sources: An upper bound. *Phys. Rev. D* **59** 023002 (1999).

12. Stein, R. Search for High-Energy Neutrinos from Populations of Optical Transients. In *36th International Cosmic Ray Conference (ICRC2019)*, volume 36 of *International Cosmic Ray Conference*, 1016 (2019).

13. Sun, H., Zhang, B. & Li, Z. Extragalactic High-energy Transients: Event Rate Densities and Luminosity Functions. *Astrophys. J.* **812** 33 (2015).

14. Stein, R., Necker, J., Bradascio, F. & Garrappa, S. IceCubeOpenSource/flarestack: Titan V2.2.3 (2020). URL https://doi.org/10.5281/zenodo.4005800.

15. Pan-Starrs Collaboration et al. Search for transient optical counterparts to high-energy IceCube neutrinos with Pan-STARRS1. *Astron. Astrophys* **626** A117 (2019).

16. Blaufuss, E. IceCube-190503A - IceCube observation of a high-energy neutrino candidate event. *GCN Circular* **24378** (2019).

17. Stein, R. et al. Optical follow-up of IceCube-190503A with ZTF. *The Astronomer's Telegram* **12730** 1 (2019).

18. Blaufuss, E. IceCube-190629A - IceCube observation of a high-energy neutrino candidate event. *GCN Circular* **24910** (2019).

19. Stein, R. et al. Optical follow-up of IceCube-190619A with ZTF. *The Astronomer's Telegram* **12879** 1 (2019).

20. Stein, R. IceCube-190730A - IceCube observation of a high-energy neutrino candidate event. *GCN Circular* **25225** (2019).

21. Stein, R. et al. Optical follow-up of IceCube-190730A with ZTF. *The Astronomer's Telegram* **12974** 1 (2019).

22. Blaufuss, E. IceCube-190922B - IceCube observation of a high-energy neutrino candidate event. *GCN Circular* **25806** (2019).

23. Stein, R., Franckowiak, A., Kowalski, M. & Kasliwal, M. A candidate supernova coincident with IceCube-190922B from ZTF. *The Astronomer's Telegram* **13125** 1 (2019).

24. Stein, R., Franckowiak, A., Kowalski, M. & Kasliwal, M. IceCube-190922B: Identification of a Candidate Supernova from the Zwicky Transient Facility. *GCN Circular* **25824** (2019).

25. Stein, R. IceCube-191001A - IceCube observation of a high-energy neutrino candidate event. *GCN Circular* **25913** (2019).

26. Stein, R., Franckowiak, A., Necker, J., Gezari, S. & Velzen, S.v. Candidate Counterparts to IceCube-191001A with ZTF. *The Astronomer's Telegram* **13160** 1 (2019).

27. Stein, R., Franckowiak, A., Necker, J. & Suvi Gezari, S.v. IceCube-191001A: Candidate Counterparts with the Zwicky Transient Facility. *GCN Circular* **25929** (2019).

28. Stein, R. IceCube-200107A: IceCube observation of a high-energy neutrino candidate event. *GCN Circular* **26655** (2020).

29. Stein, R. & Reusch, S. IceCube-200107A: No candidates from the Zwicky Transient Facility. *GCN Circular* **26667** (2020).

30. Stein, R. IceCube-200109A: IceCube observation of a high-energy neutrino candidate event. *GCN Circular* **26696** (2020).

31. Reusch, S. & Stein, R. IceCube-200109A: Candidate Counterparts from the Zwicky Transient Facility. *GCN Circular* **26747** (2020).

32. Lagunas Gualda, C. IceCube-200117A: IceCube observation of a high-energy neutrino candidate event. *GCN Circular* **26802** (2020).

33. Reusch, S. & Stein, R. IceCube-200117A: Candidate Counterpart from the Zwicky Transient Facility. *GCN Circular* **26813** (2020).

34. Reusch, S. & Stein, R. IceCube-200117A: One Additional Candidate Counterpart from the Zwicky Transient Facility. *GCN Circular* **26816** (2020).

35. Kopper, C. Retraction of IceCube GCN/AMON NOTICE 71165249_130949. *GCN Circular* **22669** (2018).

36. Blaufuss, E. IceCube-181031A retraction. *GCN Circular* **23398** (2018).

37. Blaufuss, E. Retraction of IceCube GCN/AMON NOTICE 36142391_132143. *GCN Circular* **23876** (2019).

38. Blaufuss, E. IceCube 41485283_132628.amon retraction. *GCN Circular* **24674** (2019).

39. Blaufuss, E. IceCube-180908A - IceCube observation of a high-energy neutrino candidate event. *GCN Circular* **23214** (2018).

40. Taboada, I. IceCube-181014A - IceCube observation of a high-energy neutrino candidate event. *GCN Circular* **23338** (2018).

41. Blaufuss, E. IceCube-190124A - IceCube observation of a high-energy neutrino candidate event. *GCN Circular* **23785** (2019).

42. Santander, M. IceCube-190704A - IceCube observation of a high-energy neutrino candidate event. *GCN Circular* **24981** (2019).

43. Blaufuss, E. IceCube-190712A - IceCube observation of a high-energy neutrino candidate event. *GCN Circular* **25057** (2019).

44. Santander, M. IceCube-190819A - IceCube observation of a high-energy neutrino candidate event. *GCN Circular* **25402** (2019).

45. Blaufuss, E. IceCube-191119A - IceCube observation of a high-energy neutrino candidate event. *GCN Circular* **26258** (2019).

46. Stein, R. IceCube-200227A: IceCube observation of a high-energy neutrino candidate event. *GCN Circular* **27235** (2020).

47. Stein, R. IceCube-191215A - IceCube observation of a high-energy neutrino candidate event. *GCN Circular* **26435** (2019).

48. Kopper, C. IceCube-190331A - IceCube observation of a high-energy neutrino candidate event. *GCN Circular* **24028** (2019).

49. Kopper, C. IceCube-190504A - IceCube observation of a high-energy neutrino candidate event. *GCN Circular* **24392** (2019).

50. Taboada, I. IceCube-190921A - IceCube observation of a high-energy neutrino candidate event. *GCN Circular* **23918** (2019).

51. Blaufuss, E. IceCube-190629A - IceCube observation of a high-energy neutrino candidate event. *GCN Circular* **24910** (2019).

52. Stein, R. IceCube-190922A - IceCube observation of a high-energy neutrino candidate event. *GCN Circular* **25802** (2019).

53. Blaufuss, E. IceCube-191122A - IceCube observation of a high-energy neutrino candidate event. *GCN Circular* **26276** (2019).

54. Stein, R. IceCube-191204A - IceCube observation of a high-energy neutrino candidate event. *GCN Circular* **26341** (2019).

55. Santander, M. IceCube-191231A: IceCube observation of a high-energy neutrino candidate event. *GCN Circular* **26620** (2019).

56. Lagunas Gualda, C. IceCube-200120A: IceCube observation of a high-energy neutrino candidate event. *GCN Circular* **26832** (2020).

57. Blaufuss, E. IceCube-200120A: Event likely due to background. *GCN Circular* **26874** (2020).

58. Blaufuss, E. IceCube-181023A - IceCube observation of a high-energy neutrino candidate event. *GCN Circular* **23375** (2018).

Event	R.A. (J2000) (deg)	Dec (J2000) (deg)	90% area (sq. deg.)	ZTF obs (sq. deg.)	Signalness	Ref
IC190503A	120.28	+6.35	1.94	1.37	36%	[16, 17]
IC190619A	343.26	+10.73	27.16	21.57	55%	[18, 19]
IC190730A	225.79	+10.47	5.41	4.52	67%	[20, 21]
IC190922B	5.76	-1.57	4.48	4.09	51%	[22, 23, 24]
IC191001A	**314.08**	**+12.94**	**25.53**	**20.56**	**59%**	**[25, 26, 27]**
IC200107A	148.18	+35.46	7.62	6.22	-	[28, 29]
IC200109A	164.49	+11.87	22.52	20.06	77%	[30, 31]
IC200117A	116.24	+29.14	2.86	2.66	38%	[32, 33, 34]

Table S1: **Summary of the eight neutrino alerts followed up by ZTF.** IC191001A is highlighted in bold. The 90% area column indicates the region of sky observed at least twice by ZTF, within the reported 90% localisation, and accounting for chip gaps. The *signalness* estimates the probability that each neutrino is of astrophysical origin, rather than arising from atmospheric backgrounds. One alert, IC200107A, was reported without a signalness estimate.

Cause	Events
Alert Retraction	IC180423A[35], IC181031A[36], IC190205A[37], IC190529A[38]
Proximity to Sun	IC180908A[39], IC181014A[40], IC190124A[41], IC190704A[42]
	IC190712A[43], IC190819A[44], IC191119A[45], IC200227A[46]
Low Altitude	IC191215A[47]
Southern Sky	IC190331A[48], IC190504A[49]
Poor Signalness & Localisation	IC190221A[50], IC190629A[51], IC190922A[52]
	IC191122A[53], IC191204A[54], IC191231A[55]
Bad Weather	IC200120A[56, 57]
Telescope Maintenance	IC181023A[58]

Table S2: **Summary of the 23 neutrino alerts that were not followed up by ZTF since survey start on 2018 March 20.** Of these, 4/23 were retracted, 11/23 were inaccessible to ZTF for various reasons, 6/23 were deemed alerts of poor quality, while just 2/23 were alerts that were missed although they passed our criteria.

Table S3: **Photometry for AT2019dsg, measured by *Swift*-UVOT, ZTF, LT (IOO) and SEDM.** The time (Δt) is measured in the observer frame relative to MJD 58582.8, the date of discovery for AT2019dsg.

Δt	Band	Flux [mJy]	Flux Error [mJy]	ν [10^{14} Hz]	Instrument
34.02	i	0.19	0.02	4.23	LT (IOO)
38.76	i	0.19	0.02	4.23	LT (IOO)
47.32	i	0.17	0.02	4.23	LT (IOO)
67.26	i	0.13	0.01	4.23	LT (IOO)
0.00	r	0.09	0.01	4.96	ZTF
10.45	r	0.15	0.01	4.96	ZTF
18.10	r	0.19	0.02	4.96	ZTF
23.80	r	0.20	0.02	4.96	ZTF
43.70	r	0.19	0.02	4.96	ZTF
49.43	r	0.16	0.01	4.96	ZTF
52.28	r	0.17	0.02	4.96	ZTF
55.17	r	0.15	0.01	4.96	ZTF
58.98	r	0.15	0.01	4.96	ZTF
64.65	r	0.14	0.01	4.96	ZTF
67.50	r	0.13	0.01	4.96	ZTF
71.30	r	0.11	0.01	4.96	ZTF
72.23	r	0.12	0.01	4.96	ZTF
75.03	r	0.11	0.01	4.96	ZTF
76.11	r	0.11	0.01	4.96	ZTF
77.02	r	0.12	0.01	4.96	ZTF
78.92	r	0.11	0.01	4.96	ZTF
81.71	r	0.11	0.01	4.96	ZTF
93.09	r	0.10	0.01	4.96	ZTF
97.01	r	0.10	0.01	4.96	ZTF
103.60	r	0.09	0.01	4.96	ZTF
104.62	r	0.09	0.01	4.96	ZTF

Δt	Band	Flux [mJy]	Flux Error [mJy]	ν [10^{14} Hz]	Instrument
106.44	r	0.08	0.01	4.96	ZTF
109.33	r	0.07	0.01	4.96	ZTF
115.05	r	0.07	0.01	4.96	ZTF
129.25	r	0.05	0.01	4.96	ZTF
163.38	r	0.05	0.01	4.96	ZTF
166.30	r	0.05	0.01	4.96	ZTF
167.13	r	0.05	0.00	4.96	ZTF
32.37	r	0.22	0.02	5.14	SEDM
34.01	r	0.19	0.02	5.14	LT (IOO)
38.76	r	0.17	0.02	5.14	LT (IOO)
47.32	r	0.16	0.01	5.14	LT (IOO)
23.79	g	0.20	0.02	6.67	ZTF
33.29	g	0.19	0.02	6.67	ZTF
43.76	g	0.18	0.02	6.67	ZTF
49.46	g	0.16	0.01	6.67	ZTF
49.48	g	0.17	0.02	6.67	ZTF
52.32	g	0.15	0.01	6.67	ZTF
55.16	g	0.15	0.01	6.67	ZTF
61.83	g	0.15	0.01	6.67	ZTF
64.68	g	0.12	0.01	6.67	ZTF
67.48	g	0.11	0.01	6.67	ZTF
76.06	g	0.10	0.01	6.67	ZTF
76.09	g	0.10	0.01	6.67	ZTF
78.95	g	0.10	0.01	6.67	ZTF
81.79	g	0.09	0.01	6.67	ZTF
87.48	g	0.08	0.01	6.67	ZTF
93.21	g	0.08	0.01	6.67	ZTF
100.70	g	0.08	0.01	6.67	ZTF
103.56	g	0.08	0.01	6.67	ZTF
104.59	g	0.07	0.01	6.67	ZTF
104.59	g	0.07	0.01	6.67	ZTF
104.60	g	0.07	0.01	6.67	ZTF

Δt	Band	Flux [mJy]	Flux Error [mJy]	ν [10^{14} Hz]	Instrument
104.64	g	0.07	0.01	6.67	ZTF
106.42	g	0.07	0.01	6.67	ZTF
120.79	g	0.05	0.01	6.67	ZTF
123.42	g	0.06	0.01	6.67	ZTF
135.90	g	0.04	0.00	6.67	ZTF
142.54	g	0.04	0.01	6.67	ZTF
156.79	g	0.03	0.01	6.67	ZTF
159.57	g	0.03	0.01	6.67	ZTF
163.42	g	0.03	0.00	6.67	ZTF
166.20	g	0.03	0.00	6.67	ZTF
166.22	g	0.03	0.00	6.67	ZTF
167.16	g	0.03	0.00	6.67	ZTF
168.12	g	0.03	0.00	6.67	ZTF
34.01	g	0.19	0.02	6.8	LT (IOO)
38.76	g	0.19	0.02	6.8	LT (IOO)
47.32	g	0.17	0.02	6.8	LT (IOO)
67.26	g	0.12	0.01	6.8	LT (IOO)
71.07	g	0.11	0.01	6.8	LT (IOO)
74.85	g	0.11	0.01	6.8	LT (IOO)
35.90	B	0.34	0.04	7.31	Swift-UVOT
39.59	B	0.24	0.06	7.31	Swift-UVOT
42.56	B	0.23	0.06	7.31	Swift-UVOT
45.53	B	0.22	0.06	7.31	Swift-UVOT
48.60	B	0.19	0.05	7.31	Swift-UVOT
51.21	B	0.21	0.05	7.31	Swift-UVOT
54.59	B	0.17	0.04	7.31	Swift-UVOT
67.65	B	0.26	0.06	7.31	Swift-UVOT
35.90	U	0.31	0.02	9.18	Swift-UVOT
39.59	U	0.27	0.04	9.18	Swift-UVOT
42.56	U	0.29	0.04	9.18	Swift-UVOT
45.53	U	0.31	0.03	9.18	Swift-UVOT
48.60	U	0.27	0.03	9.18	Swift-UVOT

Δt	Band	Flux [mJy]	Flux Error [mJy]	ν [10^{14} Hz]	Instrument
48.69	U	0.23	0.03	9.18	Swift-UVOT
51.02	U	0.23	0.03	9.18	Swift-UVOT
51.21	U	0.24	0.03	9.18	Swift-UVOT
54.59	U	0.23	0.02	9.18	Swift-UVOT
57.05	U	0.23	0.02	9.18	Swift-UVOT
59.89	U	0.18	0.02	9.18	Swift-UVOT
63.10	U	0.24	0.03	9.18	Swift-UVOT
67.65	U	0.18	0.03	9.18	Swift-UVOT
67.99	U	0.19	0.02	9.18	Swift-UVOT
88.18	U	0.15	0.03	9.18	Swift-UVOT
88.93	U	0.11	0.02	9.18	Swift-UVOT
93.09	U	0.11	0.02	9.18	Swift-UVOT
175.15	U	0.06	0.01	9.18	Swift-UVOT
179.76	U	0.05	0.02	9.18	Swift-UVOT
184.37	U	0.04	0.02	9.18	Swift-UVOT
35.90	UVW1	0.38	0.02	12.6	Swift-UVOT
39.59	UVW1	0.36	0.03	12.6	Swift-UVOT
42.56	UVW1	0.34	0.02	12.6	Swift-UVOT
45.52	UVW1	0.33	0.02	12.6	Swift-UVOT
48.60	UVW1	0.34	0.02	12.6	Swift-UVOT
48.69	UVW1	0.29	0.02	12.6	Swift-UVOT
51.02	UVW1	0.28	0.02	12.6	Swift-UVOT
51.21	UVW1	0.30	0.02	12.6	Swift-UVOT
54.59	UVW1	0.30	0.02	12.6	Swift-UVOT
57.05	UVW1	0.27	0.01	12.6	Swift-UVOT
59.89	UVW1	0.26	0.02	12.6	Swift-UVOT
63.10	UVW1	0.28	0.02	12.6	Swift-UVOT
67.65	UVW1	0.26	0.02	12.6	Swift-UVOT
67.99	UVW1	0.20	0.01	12.6	Swift-UVOT
88.17	UVW1	0.17	0.02	12.6	Swift-UVOT
88.93	UVW1	0.15	0.02	12.6	Swift-UVOT
93.09	UVW1	0.15	0.01	12.6	Swift-UVOT

Δt	Band	Flux [mJy]	Flux Error [mJy]	ν [10^{14} Hz]	Instrument
105.73	UVW1	0.13	0.01	12.6	Swift-UVOT
107.43	UVW1	0.11	0.01	12.6	Swift-UVOT
111.17	UVW1	0.10	0.01	12.6	Swift-UVOT
115.15	UVW1	0.11	0.01	12.6	Swift-UVOT
118.88	UVW1	0.12	0.01	12.6	Swift-UVOT
123.99	UVW1	0.09	0.01	12.6	Swift-UVOT
169.90	UVW1	0.06	0.01	12.6	Swift-UVOT
175.15	UVW1	0.06	0.01	12.6	Swift-UVOT
179.76	UVW1	0.06	0.01	12.6	Swift-UVOT
184.37	UVW1	0.04	0.01	12.6	Swift-UVOT
194.09	UVW1	0.07	0.02	12.6	Swift-UVOT
199.71	UVW1	0.07	0.01	12.6	Swift-UVOT
223.47	UVW1	0.03	0.01	12.6	Swift-UVOT
329.98	UVW1	0.03	0.01	12.6	Swift-UVOT
35.91	UVM2	0.37	0.01	14.15	Swift-UVOT
39.59	UVM2	0.35	0.02	14.15	Swift-UVOT
42.57	UVM2	0.35	0.02	14.15	Swift-UVOT
45.53	UVM2	0.35	0.02	14.15	Swift-UVOT
48.60	UVM2	0.32	0.01	14.15	Swift-UVOT
48.69	UVM2	0.33	0.02	14.15	Swift-UVOT
51.03	UVM2	0.26	0.01	14.15	Swift-UVOT
51.22	UVM2	0.29	0.02	14.15	Swift-UVOT
54.60	UVM2	0.28	0.01	14.15	Swift-UVOT
57.06	UVM2	0.28	0.01	14.15	Swift-UVOT
59.90	UVM2	0.26	0.01	14.15	Swift-UVOT
63.10	UVM2	0.25	0.01	14.15	Swift-UVOT
67.65	UVM2	0.26	0.02	14.15	Swift-UVOT
68.00	UVM2	0.20	0.01	14.15	Swift-UVOT
88.18	UVM2	0.15	0.01	14.15	Swift-UVOT
88.94	UVM2	0.18	0.01	14.15	Swift-UVOT
93.10	UVM2	0.13	0.01	14.15	Swift-UVOT
105.72	UVM2	0.12	0.01	14.15	Swift-UVOT

Δt	Band	Flux [mJy]	Flux Error [mJy]	ν [10^{14} Hz]	Instrument
107.43	UVM2	0.10	0.01	14.15	Swift-UVOT
111.16	UVM2	0.10	0.01	14.15	Swift-UVOT
115.15	UVM2	0.10	0.01	14.15	Swift-UVOT
118.87	UVM2	0.09	0.01	14.15	Swift-UVOT
123.99	UVM2	0.07	0.01	14.15	Swift-UVOT
169.91	UVM2	0.05	0.01	14.15	Swift-UVOT
175.16	UVM2	0.04	0.00	14.15	Swift-UVOT
179.77	UVM2	0.05	0.01	14.15	Swift-UVOT
184.38	UVM2	0.04	0.01	14.15	Swift-UVOT
194.09	UVM2	0.05	0.01	14.15	Swift-UVOT
199.72	UVM2	0.04	0.01	14.15	Swift-UVOT
223.48	UVM2	0.04	0.01	14.15	Swift-UVOT
329.97	UVM2	0.01	0.00	14.15	Swift-UVOT
35.90	UVW2	0.52	0.01	15.69	Swift-UVOT
39.59	UVW2	0.47	0.03	15.69	Swift-UVOT
42.56	UVW2	0.43	0.02	15.69	Swift-UVOT
45.53	UVW2	0.41	0.02	15.69	Swift-UVOT
48.60	UVW2	0.42	0.02	15.69	Swift-UVOT
48.69	UVW2	0.44	0.02	15.69	Swift-UVOT
51.02	UVW2	0.40	0.02	15.69	Swift-UVOT
51.21	UVW2	0.39	0.02	15.69	Swift-UVOT
54.59	UVW2	0.38	0.01	15.69	Swift-UVOT
57.05	UVW2	0.36	0.01	15.69	Swift-UVOT
59.89	UVW2	0.36	0.01	15.69	Swift-UVOT
63.10	UVW2	0.32	0.02	15.69	Swift-UVOT
67.65	UVW2	0.29	0.02	15.69	Swift-UVOT
68.00	UVW2	0.31	0.01	15.69	Swift-UVOT
88.18	UVW2	0.23	0.01	15.69	Swift-UVOT
88.93	UVW2	0.21	0.01	15.69	Swift-UVOT
93.10	UVW2	0.20	0.01	15.69	Swift-UVOT
105.72	UVW2	0.17	0.01	15.69	Swift-UVOT
107.43	UVW2	0.13	0.01	15.69	Swift-UVOT

Δt	Band	Flux [mJy]	Flux Error [mJy]	ν [10^{14} Hz]	Instrument
111.16	UVW2	0.12	0.01	15.69	Swift-UVOT
115.15	UVW2	0.15	0.01	15.69	Swift-UVOT
118.87	UVW2	0.13	0.01	15.69	Swift-UVOT
123.98	UVW2	0.10	0.01	15.69	Swift-UVOT
169.90	UVW2	0.06	0.01	15.69	Swift-UVOT
175.15	UVW2	0.06	0.00	15.69	Swift-UVOT
179.77	UVW2	0.06	0.01	15.69	Swift-UVOT
184.38	UVW2	0.07	0.01	15.69	Swift-UVOT
194.09	UVW2	0.06	0.01	15.69	Swift-UVOT
199.72	UVW2	0.04	0.01	15.69	Swift-UVOT
223.47	UVW2	0.06	0.01	15.69	Swift-UVOT
329.96	UVW2	0.02	0.00	15.69	Swift-UVOT

Table S4: **X-ray observations of AT2019dsg from *Swift-XRT* and *XMM-Newton*.** The time (Δt) is measured in the observer frame relative to MJD 58582.8. After $\Delta t = 65.96$, the source was not detected. For these observations, we instead report 3σ upper limits.

Δt	Energy Flux [10^{-12} erg cm^{-2} s^{-1}]	Flux Err [10^{-12} erg cm^{-2} s^{-1}]	Energy Range [keV]	Instrument
37.37	4.27	0.42	0.3-10	Swift-XRT
41.24	1.27	0.67	0.3-10	Swift-XRT
44.37	1.97	0.46	0.3-10	Swift-XRT
47.48	3.45	0.61	0.3-10	Swift-XRT
50.16	1.56	0.04	0.3-10	XMM-Newton
50.75	2.40	0.34	0.3-10	Swift-XRT
53.36	1.30	0.26	0.3-10	Swift-XRT
57.01	0.18	0.10	0.3-10	Swift-XRT
59.6	0.78	0.23	0.3-10	Swift-XRT
62.59	0.38	0.15	0.3-10	Swift-XRT
65.96	0.49	0.23	0.3-10	Swift-XRT
70.94	0.37	-	0.3-10	Swift-XRT
92.72	0.46	-	0.3-10	Swift-XRT
97.49	0.34	-	0.3-10	Swift-XRT
110.76	0.78	-	0.3-10	Swift-XRT
112.56	0.96	-	0.3-10	Swift-XRT
116.48	0.79	-	0.3-10	Swift-XRT
120.67	0.64	-	0.3-10	Swift-XRT
124.59	0.66	-	0.3-10	Swift-XRT
129.96	0.84	-	0.3-10	Swift-XRT
146.44	2.99	-	0.3-10	Swift-XRT
149.09	0.98	-	0.3-10	Swift-XRT
150.64	0.81	-	0.3-10	Swift-XRT
178.23	0.66	-	0.3-10	Swift-XRT

Δt	Energy Flux [10^{-12} erg cm^{-2} s^{-1}]	Flux Err [10^{-12} erg cm^{-2} s^{-1}]	Energy Range [keV]	Instrument
183.68	0.30	-	0.3-10	Swift-XRT
196.16	0.09	-	0.3-10	XMM-Newton

Table S5: Radio observations of AT2019dsg from MeerKAT, VLA, and AMI-LA, grouped into quasi-simultaneous epochs. The time (Δt) is measured in the observer frame relative to MJD 58582.8, the date of discovery for AT2019dsg.

Δt	ν [GHz]	Flux density [mJy]	Flux Err [mJy]	Instrument
42	8.49	0.290	0.032	VLA
42	9.51	0.408	0.035	VLA
42	10.49	0.440	0.036	VLA
42	11.51	0.412	0.037	VLA
41	15.50	0.464	0.045	AMI
70	1.28	0.104	0.018	MeerKAT
70	3.50	0.103	0.028	VLA
70	4.49	0.319	0.040	VLA
70	5.51	0.324	0.033	VLA
70	6.49	0.443	0.037	VLA
70	7.51	0.558	0.041	VLA
70	8.49	0.680	0.045	VLA
70	9.51	0.730	0.047	VLA
70	10.49	0.756	0.048	VLA
70	11.51	0.771	0.051	VLA
71	15.50	0.730	0.076	AMI
111	1.28	0.111	0.017	MeerKAT
120	2.24	0.249	0.065	VLA
120	2.76	0.345	0.053	VLA
120	3.18	0.255	0.049	VLA
120	3.69	0.419	0.043	VLA
120	4.74	0.698	0.046	VLA
120	5.76	0.829	0.053	VLA
120	6.69	0.987	0.058	VLA
120	7.71	1.117	0.063	VLA
120	8.49	1.194	0.067	VLA

Δt	ν [GHz]	Flux density [mJy]	Flux Err [mJy]	Instrument
120	9.51	1.238	0.069	VLA
120	10.14	1.310	0.073	VLA
120	11.16	1.356	0.075	VLA
119	15.50	0.978	0.075	AMI
179	1.28	0.152	0.019	MeerKAT
178	2.24	0.351	0.055	VLA
178	2.75	0.744	0.054	VLA
178	3.24	0.920	0.057	VLA
178	3.76	1.032	0.063	VLA
178	4.74	1.349	0.073	VLA
178	5.76	1.379	0.075	VLA
178	6.69	1.285	0.071	VLA
178	7.71	1.111	0.062	VLA
178	8.49	1.074	0.062	VLA
178	9.51	0.921	0.054	VLA
178	10.14	0.884	0.053	VLA
178	11.16	0.785	0.049	VLA
179	15.50	0.676	0.055	AMI
235	1.28	0.178	0.032	MeerKAT
236	15.50	0.503	0.047	AMI